

University of Dundee

## Investigation of Long Waves Generated by Bottom-Tilting Wave Maker

Lu, Heng; Park, Yong Sung; Cho, Yong Sik

*Published in:*  
Coastal Engineering Journal

*DOI:*  
[10.1142/S0578563417500188](https://doi.org/10.1142/S0578563417500188)

*Publication date:*  
2017

*Licence:*  
Other

*Document Version*  
Peer reviewed version

[Link to publication in Discovery Research Portal](#)

*Citation for published version (APA):*  
Lu, H., Park, Y. S., & Cho, Y. S. (2017). Investigation of Long Waves Generated by Bottom-Tilting Wave Maker. *Coastal Engineering Journal*, 59(4), 1-23. [1750018]. <https://doi.org/10.1142/S0578563417500188>

### General rights

Copyright and moral rights for the publications made accessible in Discovery Research Portal are retained by the authors and/or other copyright owners and it is a condition of accessing publications that users recognise and abide by the legal requirements associated with these rights.

- Users may download and print one copy of any publication from Discovery Research Portal for the purpose of private study or research.
- You may not further distribute the material or use it for any profit-making activity or commercial gain.
- You may freely distribute the URL identifying the publication in the public portal.

### Take down policy

If you believe that this document breaches copyright please contact us providing details, and we will remove access to the work immediately and investigate your claim.

## Investigation of Long Waves Generated by Bottom-Tilting Wave Maker

Heng Lu

*School of Science and Engineering, University of Dundee, Perth Road  
 Dundee, DD1 4HN, United Kingdom  
 h.z.lu@dundee.ac.uk*

Yong Sung Park \*

*School of Science and Engineering, University of Dundee, Perth Road  
 Dundee, DD1 4HN, United Kingdom  
 y.s.park@dundee.ac.uk*

Yong-Sik Cho

*Civil and Environmental Engineering, Hanyang University, 222 Wangsimni-ro  
 Seoul, 133-791, Republic of Korea  
 ysc59@hanyang.ac.kr*

Received (Day Month Year)

Revised (Day Month Year)

Motivated by recent field observations of tsunamis, a new wave maker, namely bottom-tilting wave maker, has been designed and investigated in order to generate very long waves in the laboratory. Theoretical results from the linear wave theory and the numerical modelling based on the weakly nonlinear and weakly dispersive wave theory show good agreement with the measurements. Using both theoretical and experimental results, the relation between the bottom motion and the resulting waves have been investigated. Wave amplitude and period of the generated waves are the subject of the parametric analysis, which verifies that the wave maker is able to generate waves longer than the effective wavelength of the solitary wave with the same wave amplitude.

**Keywords:** Long waves; wave maker; Boussinesq equations; nonlinear shallow equations; linear wave theory.

### 1. Introduction

Tsunamis can be caused by undersea earthquakes, such as the recent tragic events including the 2004 Indian tsunami, the 2011 Tohoku tsunami and the 2015 Chile tsunami [Tsuji *et al.*, 2006; Hayashi *et al.*, 2011; Aránguiz *et al.*, 2016]. They can have extremely long wavelengths and very small amplitudes compared to ocean depths [Mei, 1989]. It is of great importance to build an appropriate physical wave model in tsunami research for more accurate theoretical and experimental investigations. Over the past few decades, solitary

\*Corresponding author.

35 waves have been extensively used as model tsunami [e.g. Hall and Watts, 1953; Hammack,  
36 1973; Synolakis, 1987; Li and Raichlen, 2002]. A solitary wave propagates in constant  
37 depth with permanent form, whose surface elevation is described as

$$\eta'(x', t') = A'_s \text{sech}^2 [K'_s(x' - c't')] , \quad K'_s = \frac{1}{h'_0} \sqrt{\frac{3A'_s}{4h'_0}}, \quad (1)$$

38 in the horizontal coordinate  $x'$  and time  $t'$ , where  $\eta'$ ,  $A'_s$ ,  $c'$  and  $h'_0$  denote free surface ele-  
39 vation, wave height, phase velocity and static water depth, respectively. Boussinesq [1872]  
40 first developed the wave profile which is also the exact solution of the Korteweg–de Vries  
41 (KdV) equation. Owing to the solid theoretical foundation, solitary waves have become  
42 popular in tsunami science. The fact that the generation of a solitary wave is relatively  
43 straightforward [Goring, 1978] might be another reason why they have attracted interests  
44 from many researchers .

45 However, recent research [e.g. Madsen *et al.*, 2008] has questioned the relevance of  
46 solitary wave in tsunami research as the link between its wavenumber  $K'_s$  and wave height  
47  $A'_s$  is not realistic for geophysical tsunamis. The real-time field records of the 2011 Japan  
48 Tohoku tsunami outlined in Fujii *et al.* [2011] clearly show that the effective wavelength  
49 of the solitary wave is an order-of-magnitude short and the wave front is too steep when  
50 compared to the observed leading tsunami. Note that we define the effective wave length  $L'_s$   
51 of a solitary wave as  $L'_s = 2\pi/K'_s$ .

52 There have been many types of wave makers that have been developed, among which  
53 piston-type wave makers are commonly used to generate long waves [e.g. Li and Raichlen,  
54 2002; Fujima *et al.*, 2009; Lo *et al.*, 2013; Schimmels *et al.*, 2016]. Piston-type wave makers  
55 can create approximately uniform flow field in the vertical direction, which is an important  
56 characteristic of long waves. However, as illustrated in figure 1, the wavelength of the gen-  
57 erated waves is limited by the stroke length  $L'_p$ .

58 On the other hand, Hammack [1973] developed a bottom-moving wave maker to create  
59 solitary waves excited by vertical bottom motions. He also found that solitary waves were  
60 generated by positive bed motion while negative waves were generated by negative bed  
61 motion. After some distance (e.g., 180 times the still water depth) , the positive waves de-  
62 veloped into a train of solitary waves which were ordered by amplitude, and negative waves  
63 developed into a dispersive train of waves. As Hammack [1973] pointed out, however, the  
64 wavelength is largely determined by the length of the moving bottom, and the resulting  
65 waves were still shorter than tsunamis.

66 Dam-break bores have also been used in laboratory experiments [e.g. O'Donoghue  
67 *et al.*, 2010; Kihara *et al.*, 2015]. O'Donoghue *et al.* [2010] used a dam-break rig to model  
68 a swash event of a turbulent bore by rapidly lifting a gate and releasing water stored behind  
69 the gate. A Large-scale Tsunami Physical Simulator was utilised by Kihara *et al.* [2015]  
70 to generate a tsunami bore traveling over a dry bed to investigate the pressure on a vertical  
71 tide wall by controlling a radial gate and the water height in the overhead tank.

72 Moreover, Rossetto *et al.* [2011] used a pneumatic-type wave maker to create long  
73 waves by releasing a volume of water into wave basin in a controlled manner. Goseberg

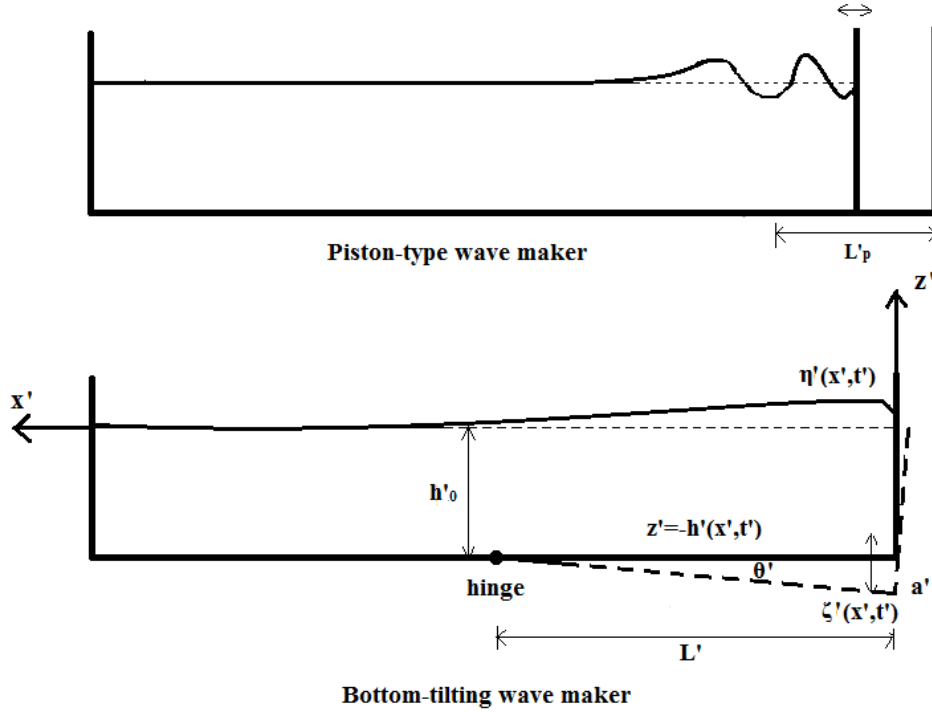


Fig. 1. Comparison between piston-type wave maker and the bottom-tilting wave maker.

74 *et al.* [2013] investigated pump-driven long wave generation in a closed-circuit wave flume,  
 75 which successfully generated long waves resembling tsunamis. While it is encouraging that  
 76 these novel wave makers are not limited by the stroke length, it is not easy to develop  
 77 theories for these new types of wave makers due to their unusual boundary conditions.

78 In order to make much longer waves in laboratory, perhaps a straightforward idea would  
 79 be moving the entire bottom and generating waves as long as the tank itself. In the present  
 80 research, a tilting bottom was used, as the simplicity of the design was attractive. Therefore,  
 81 the new wave maker used in this study was designed based on the concept depicted in  
 82 figure 1. In comparison with the typical piston-type wave maker, the bottom tilting wave  
 83 maker has a much longer moving part with length  $L'$ , which can thus produce longer waves.  
 84 Unlike the disintegration of the waves observed in Hammack [1973]'s study, the generated  
 85 wave will be used immediately before it disintegrates into a train of shorter waves. The long  
 86 wave will soon run up the adjustable beach which is directly hinged to the moving bottom.

87 Recently, Lu *et al.* [2017] provided the theoretical foundation needed in controlling the  
 88 new wave maker. In the present paper, using a combined methodology, including linear and  
 89 nonlinear solutions as well as experimental measurements, we aim to verify that the new  
 90 wave maker is able to create long waves through a comparison of the effective wavelengths  
 91 between the generated long waves and solitary waves and to explore its capacity of mod-

elling real tsunamis. Furthermore, we investigate the relation between the bottom motion and the resulting wave, expecting to describe the generated waves in terms of its generation parameters.

The rest of the article is organized as follows. For completeness, the theoretical background is briefly reviewed in Section 2. The preliminary design of a bottom-tilting wave maker based on the linear wave theory is introduced in Section 3. Section 4 provides the details of the wave maker and the corresponding experimental procedures. Theoretical and experimental results are compared to each other in Section 5, and the relationship between the bottom motion and the resulting waves is sought. Further discussion on the waves generated by bottom-tilting wave maker are presented in Section 6. Finally, concluding remarks are given in Section 7.

## 2. Theoretical background

A schematic sketch of the two-dimensional wave tank is depicted in figure 1 with the corresponding coordinate system. Lu *et al.* [2017] provided the analytical solution of the free surface elevation by solving the two-dimensional Laplace equation along with the specific boundary conditions derived from the linear wave theory. The free surface elevation  $\eta'(x, t)$  is given by

$$\eta'(x' = L', t') = \frac{a' L'}{\pi} \int_0^{t'} du' \int_0^\infty dk' \frac{\sin^2(k' L'/2)}{(k' L'/2)^2} \frac{\cos k' L'}{\cosh k' h'_0} Q'(u') \cos \omega' (t' - u'), \quad (2)$$

with the bottom motion displacement  $\zeta'$  given by

$$\zeta'(x', t') = D'_0(x') T'(t'), \quad (3)$$

and

$$Q'(t') = \frac{d}{dt'} T'(t'), \quad (4)$$

where  $a'$  and  $h'_0$  denote the motion amplitude at the right end of the tilting bottom and constant water depth, respectively.  $D'_0(x)$  describes the shape of the moving bottom, which is given as for flat bottom of length  $L'$

$$D'_0(x') = \begin{cases} a'(1 - |x'|/L'), & |x'| \leq L', \\ 0, & \text{otherwise,} \end{cases} \quad (5)$$

The wavenumber  $k'$  and the frequency  $\omega'$  are related by the dispersion relation  $\omega'^2 = g' k' \tanh k' h'_0$ . Note that the flow is assumed to be inviscid, incompressible and irrotational.

We remark here that the analytical solution Eq. (2) is obtained for an infinite domain. Therefore comparison between Eq. (2) and the experimental results will be only valid in the early stages of the experiments when the reflected wave from the other end has not affected the incident wave.

The weakly dispersive and weakly nonlinear wave theory is also used to model the wave maker. The Boussinesq equations (BE) derived by Wu [1987] are written in conservative form as shown below:

$$\left. \begin{aligned} H'_{t'} + [H'u']_{x'} &= 0, \\ u'_{t'} + [\frac{1}{2}u'^2 + g'(H' - h')]_{x'} &= \frac{1}{2}h'h'_{x't't'} + \frac{1}{2}h'(h'u')_{x'x't'} - \frac{1}{6}h'^2u'_{x'x't'}, \end{aligned} \right\} \quad (6)$$

where the subscript  $t$  and  $x$  indicate temporal and spatial derivatives, respectively, the total water depth  $H' = \eta' + h'$ , and  $h'$  and  $u'$  denote the water depth under the static water line and the horizontal velocity, respectively. According to Lu *et al.* [2017], Eq. (6) can be rearranged as shown below:

$$\mathbf{V}_{t'} + [\mathbb{F}(\mathbf{V})]_{x'} = \mathbb{S}_b + \mathbb{M}(\mathbf{V}), \quad (7)$$

where the variable  $\mathbf{V}$ , the advective flux  $\mathbb{F}(\mathbf{V})$ , the source term  $\mathbb{S}_b$  and the dispersive term  $\mathbb{M}(\mathbf{V})$  are denoted respectively by  $\mathbf{V} = \begin{pmatrix} H' \\ u' \end{pmatrix}$ ,  $\mathbb{F}(\mathbf{V}) = \begin{pmatrix} H'u' \\ \frac{1}{2}u'^2 + g'(H' - h') \end{pmatrix}$ ,  $\mathbb{S}_b = \begin{pmatrix} 0 \\ \frac{1}{2}h'h'_{x't't'} \end{pmatrix}$  and  $\mathbb{M}(\mathbf{V}) = \begin{pmatrix} 0 \\ \frac{1}{2}h'(h'u')_{x'x't'} - \frac{1}{6}h'^2u'_{x'x't'} \end{pmatrix}$ . They can be simplified by omitting the dispersive terms and become the nonlinear shallow water equations (NSWE). The equations are solved by a shock-capturing finite volume method with high-order reconstruction schemes [Lu *et al.*, 2017], so that the discontinuities at cell interfaces in the discrete solution are treated by higher-order approximations, such as second-order-accurate UNO2 [Harten and Osher, 1987], third-order-accurate WENO3 and fifth-order-accurate WENO5 [Shu, 1998]. In practice, UNO2 is used for the Boussinesq equations system, while WENO schemes are used for the nonlinear shallow water equations system. The analysis in section 5 is based on the BE system, while the NSWE system will be compared with the BE system to demonstrate the effects of the dispersion. A semi-infinite computational is used to obtain the wavelength and the back profile of the generated waves. In all the other cases, the computational analysis is based on the confined domain, identical to the physical wave tank with full reflective boundaries considered.

In this study, the bottom motion is of finite duration, which can excite the fluid and produce transient waves. For simplicity, only the bottom motions with constant velocity for given duration are considered as shown below:

$$Q'(t') = \begin{cases} 1/b', & 0 \leq t' \leq b' & \text{upward motion,} \\ -1/b', & 0 \leq t' \leq b' & \text{downward motion,} \end{cases} \quad (8)$$

where  $b'$  denotes the motion duration time. More complex bottom motions are also possible, for example the resulting wave shown by a dashed line in figure 12 which will be discussed later. As the duration of the bottom motion increases, however, the effects of reflected waves become dominant, especially in the wave tank with a limited length. Therefore, more general motions are left as future studies when the challenges of dealing with reflected waves are fully addressed.

In the following discussions, results are described in terms of dimensionless variables. The constant water depth  $h'_0$  is used to normalise the length parameters, so the relevant dimensionless variables are given by

$$L = \frac{L'}{h'_0}, x = \frac{x'}{h'_0}, h' = \frac{h'}{h'_0}, \eta = \frac{\eta'}{h'_0}, \zeta = \frac{\zeta'}{h'_0}, a = \frac{a'}{h'_0}, A = \frac{A'}{h'_0}, \quad (9)$$

while time is normalised by  $L' / \sqrt{g'h'_0}$

$$t = t' \sqrt{g'h'_0/L'}, b = b' \sqrt{g'h'_0/L'}, T = T' \sqrt{g'h'_0/L'}, \quad (10)$$

where  $L'$ ,  $A'$  and  $T'$  denote the length of the tilting bottom, the wave amplitude and the wave period, respectively. Moreover, as the length of the moving bottom is fixed in reality,  $\alpha = h'_0/L'$  can be used to represent the constant water depth, in some cases discussed later.

### 3. Preliminary design

As can be seen in figure 1, the wave maker consists of a moving bottom hinged to a fixed bottom, so that the bottom will move in a rotational motion with the vertical displacement of the moving part  $\zeta(x, t) \approx (L - x)\theta(t)$ . The moving bottom part will generate long waves, and the other part is for the generated waves to propagate in the constant water depth or to run up the slope. The origin of the coordinate system is at the right end of the static water surface with  $x$  axis pointing leftwards and  $z$  axis pointing upwards. The fluid domain is bounded by the two end walls, the free surface  $z = \eta(x, t)$  and the solid impermeable bottom boundary  $z = -h(x, t)$ . Note that  $h(x, t) = 1 - \zeta(x, t)$  with  $h_0 = 1$ .

Our purpose in this section is to demonstrate that the wave maker with the specific geometry is capable of generating waves longer than solitary waves. Then, the ratio  $\alpha$  is of interest for limiting the generation of long waves and is discussed by considering the linear wave theory (2). It can be found that the wavelength increases with growing motion duration, so that the minimum and observable duration time (0.5 s) the actuator can provide is used to generate the shortest wave for the following cases discussed. It is also remarked here that, as the analytical solution for downward motion is just opposite to that for upward motion, it is efficient to use only upward motion for design purposes. Moreover, both motions begin from the initial position where  $\theta \neq 0$  and stop at  $\theta = 0$  to ensure flat bottom throughout the wave tank for wave propagation, and slope is not considered here.

Based on the typical relation of  $\alpha = O(0.1)$ , a range of water depths  $\alpha$  and the bottom motion amplitudes  $a$  are tested as shown in figure 2. The analytical solution (2) was used to compare the ratio  $L_w/L_s$  indicating the ability of the wave maker of generating waves longer than the solitary waves, where  $L_s$  is the solitary wave length and  $L_w$  is the generated wave length. It is observed in figure 2 that  $L_w/L_s$  grows with decreasing  $\alpha$  and with increasing  $a$ . For the smallest  $a = 0.1$  tested here, it is expected that the generated wave will be longer than the solitary wave for  $\alpha < 0.07$ .

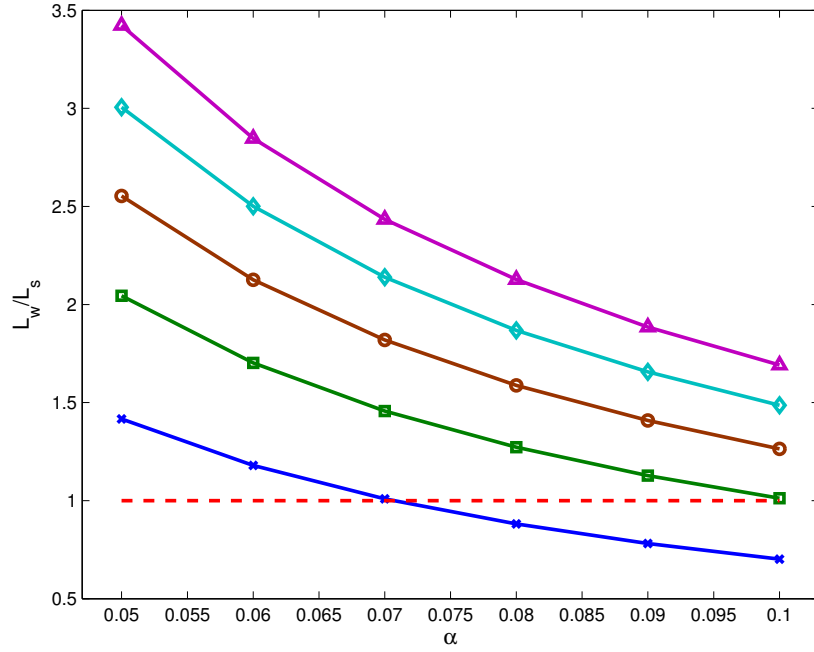


Fig. 2. The ratios of the generated wave length to the solitary wave length,  $L_w/L_s$ , plotted against varying  $\alpha$  and  $a$ : ---,  $L_w/L_s = 1$ ; +,  $a = 0.1$ ; □,  $a = 0.2$ ; ○,  $a = 0.3$ ; ◇,  $a = 0.4$ ; △,  $a = 0.5$ .

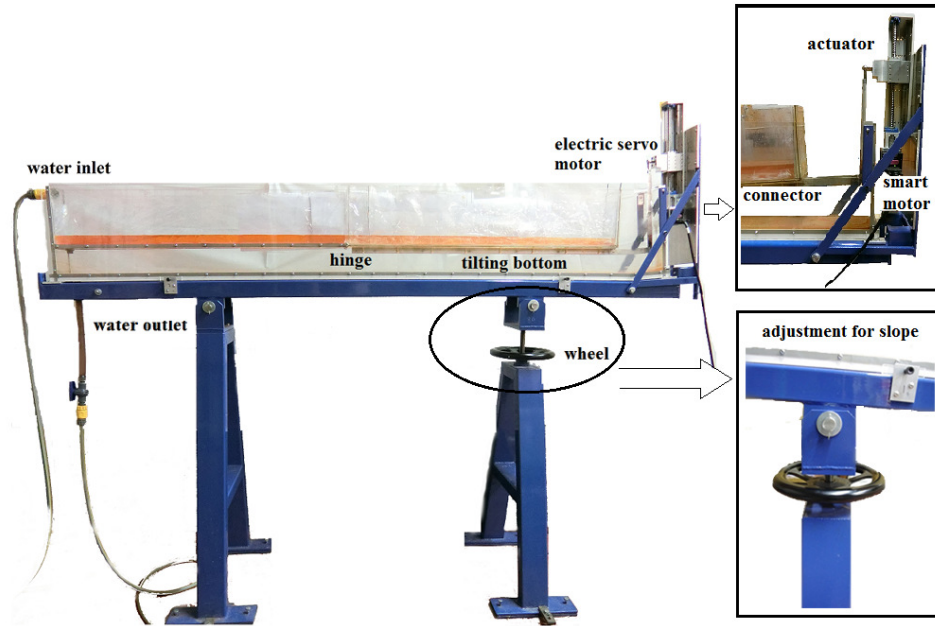
#### 4. Experimental equipment and procedures

A series of experiments was carried out in the wave tank shown in figure 3, which also presents the set-up of the experiments. The tank is 2.185 m long, 0.11 m wide and 0.3 m deep, and consists of an adjustable slope and the bottom-tilting wave maker. The wave tank is regarded as being two-dimensional, so that the resulting waves are also two-dimensional. The bottom-tilting wave generator has a 1 m long and 0.11 m wide moving bottom which is hinged to the slope which has the same dimensions. The hinge is located at 0.2 m below the top of the tank, which leaves enough space for varying bottom motions (upward, downward or combination).

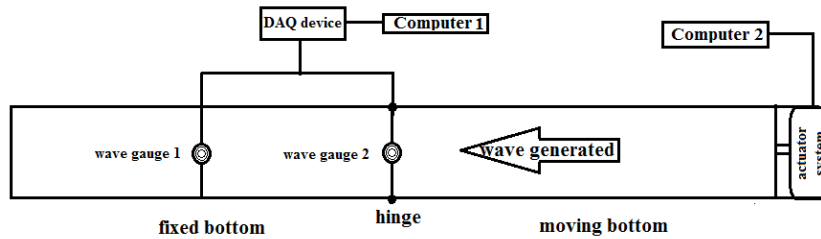
The moving bottom is controlled by an ANIMATICS® SM23165DT electrical servo motor located at the right end of the tank which has a rotating rod to move the actuator. The actuator moves vertically under the command of the programme called SmartMotor™ Interface, and it provides the moving bottom with the prescribed vertical velocity and displacement directly through a steel connector attached to the back of the bottom.

Rubber seals were attached around the moving bottom. In addition, a 2.3 m long and 0.31 m wide PVC membrane covers the inner surface of the wave tank to ensure water-proofness. The whole wave tank is supported by two legs, and there is a wheel on the right leg used for adjusting the slope of the fixed bed. Then, the beach with desired slope was





(a) Photo of the bottom-tilting wave maker (components are shown as indicated)



(b) Plot of the set-up

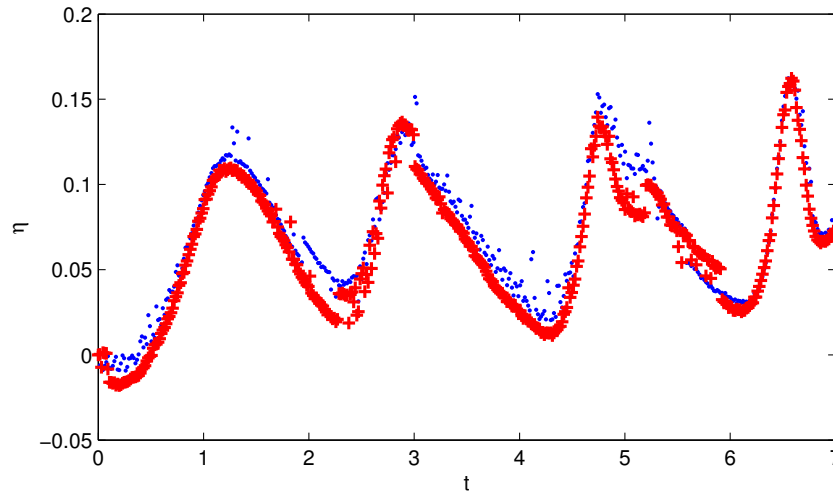
Fig. 3. Set-up of the bottom-tilting wave maker.

created by a specific height difference. In the present study, the fixed bottom was always flat.

Two acoustic wave gauges (BANNER® U-STAGE™S18UUA) were used to measure the free surface elevation at the hinge (1 m from the right end) and middle of the fixed bottom (1.5 m from the right end) as shown in figure 3 (b), respectively. The two wave gauges are ultrasonic sensors with analog output relying on time-varying voltage proportional to the time history of the displacement. The measurement frequency was set to be 50 Hz and measurement duration time 10 s which begins with the bottom motion, and is sufficient to measure the time history of the free surface elevation. The accuracy of the gauges is  $\pm 0.5$  mm. Data is collected by a computer through a National Instruments™ Low-Cost

Table 1. Normalised bottom motion parameters ( $a$  and  $b$ ) of the bottom motions for different  $\alpha$ .

$\alpha$	$a$	$b$
0.04	0.125, 0.250 $\cdots$ , 1.000	0.3132, 0.6264, 0.9396, 1.2528
0.05	0.100, 0.200 $\cdots$ , 0.800	0.3502, 0.7004, 1.0505, 1.4007
0.06	0.083, 0.167 $\cdots$ , 0.677	0.3836, 0.7672, 1.1508, 1.5344

Fig. 4. Comparison of two repetitions of the time history of  $\eta$  at the hinge.

212 USB Data Acquisition (DAQ) 6003.

213 Motion displacement  $a$  and duration time  $b$  are the two defining parameters of the basic  
 214 upward or downward bottom motion. Limited by the maximum value of the ratio  $\alpha$  being  
 215 0.07, three values 0.04, 0.05 and 0.06 were tested. After some trials, the maximum allow-  
 216 able bottom motion displacement without causing splash-up at the end wall was found to  
 217 be under  $a=1$ , 0.8 and 0.677 for the three different  $\alpha$ , respectively. On the other hand, the  
 218 corresponding rotating angle would be  $0.013\pi$ , which is small enough to ignore the hor-  
 219 izontal velocity induced by the moving bottom as long as the bottom motion is not very  
 220 strong. Thus, the bottom motion displacement within the range of 0.083 to 1 were chosen  
 221 in this study. Moreover, bottom motion duration time ranges from  $b=0.3$  to 1.5. Ranges of  
 222 the normalized parameters used in the experiments are summarized in Table 1. Experiments  
 223 are repeated a second time to ensure repeatability. For example, figure 4 shows two repe-  
 224 titions of the time history of the free surface elevation at the hinge. There are only small  
 225 differences between the two measurements, and the error is within the accuracy of the wave  
 226 gauge ( $\pm 0.01$ ).

## 5. Experimental results

The purpose of the present study is to relate the wave amplitude  $A$  and the wave period  $T$  of the waves generated in the new wave tank in terms of the two parameters ( $a$  and  $b$ ) of the simple upward and downward motions in Eq. (8) and (3). Firstly, the authors will demonstrate that there is good agreement between experimental and theoretical results for all the cases in Table 1, even with the multiple reflections on both ends of the tank. It is straightforward to get  $A$  from experimental data, but  $T$  is more difficult to measure due to the presence of the reflected wave. Instead, the authors use theoretical solutions in semi-infinite domain to estimate  $T$ . It is noted here that the cases shown in this section are for  $\alpha = 0.05$  if not specified otherwise, but similar results were observed in the other cases as well.

### 5.1. Comparison of experimental and theoretical results

The numerical results of the time-histories of the free surface elevation at the hinge are compared to the experimental data, and examples are shown in figure 5 covering a wide range of bottom motion amplitude  $a$  and duration  $b$ . For small  $a$ , the wave amplitude is small and sometimes comparable to the uncertainty (0.5 mm) of the wave gauges, which resulted in scattering of the experimental data for  $a = 0.2$  in figure 5. Nevertheless, both the Boussinesq equations and the nonlinear shallow water equations show good agreement with the experimental data. Eventually dispersion becomes no longer negligible, and the Boussinesq equations capture it well. It is also observed that the resulting waves become increasingly asymmetric with greater motion displacement because of the growing nonlinearity, in particular the negative waves. In addition, it can be found that the wave amplitudes of the resulting waves are smaller than the corresponding motion displacement, roughly half as much as the relevant motion amplitude for most cases.

### 5.2. Wave amplitudes of the waves generated using the bottom-tilting wave maker

The amplitudes of the waves generated in the new wave tank are plotted as a function of the bottom motion displacement  $a$  and the duration  $b$  in figure 6. The amplitude was defined by the elevation of the first peak for the positive waves or the first trough for the negative waves. It is observed that greater motion displacement  $a$  and smaller bottom motion duration  $b$  leads to increasing wave amplitude  $A$  for both upward and downward motions. However, effects of the motion duration on the wave amplitude become less important for downward motions as the motion amplitude increases. This suggests that early disintegration of the high-amplitude leading depression wave caused by dispersion plays a role in determining the wave amplitude of negative waves.

In an effort to succinctly describe the wave amplitude in terms of  $a$  and  $b$ , it is instructive to consider scaling analysis. In their experimental study of tsunami generation due to subaerial mass flow, Walder *et al.* [2003] argued that amplitude of tsunami is mainly a function of volume flux of displaced water. In the present research, the volume (per unit width) of displaced water in the bottom-tilting wave maker is  $V_w = aL/2$ , which was in motion

Table 2. Parameters ( $m$  and  $n$ ) of the fitting functions for different bottom motion type.

motion type	$m$	$n$
upward	0.06547	0.4994
downward	0.09224	0.4380

for the duration of  $b$ . Following Walder *et al.* [2003], wave amplitudes measured from the experiments are plotted against the inverse of the volume flux, that is  $b/V_w$ , in figure 7. The two fitting functions are of form  $A = m(b/V_w)^{-n}$ , and the results are summarised in Table 2. Walder *et al.* [2003] reported  $m = 1.32$  and  $n = 0.68$ . On the other hand, the values of  $m$  for our experimental data are smaller, possibly because of the different time normalization, different generation mechanism and absence of acceleration for most of the bottom displacement.

### 5.3. Estimation of wave period

Due to the limited length of the wave tank, the reflected wave makes measuring  $T$  rather difficult. Two different methods were employed to estimate the wave periods. One is to measure time from the beginning of the wave to the peak of the wave, namely wave peak time  $T_a$ , in which the beginning is defined as the point where the water surface elevation is 1% of the wave amplitude. Then the wave period is estimated to be  $T = 2T_a$ . This method, however, works only for the waves that are more or less symmetric. Waves generated using the bottom-tilting wave maker becomes increasingly skewed as the  $ab^{-1}$  grows. In those cases, theoretical solutions in semi-infinite domain are used instead. Figure 8 presents the comparison between the theoretical results for  $a = 0.5$  and  $b = 0.70$  and the experimental data up to the arrival of the reflected wave. Both the Boussinesq equations and the nonlinear shallow water equations show good agreement with the experimental data before they are affected by the reflected wave. On the other hand, the linear analytic solution is quite different from the data, which means that nonlinear effects of the deformation of the wave profile are not negligible in wave generation. Using the numerical results from the Boussinesq equations in semi-infinite domain, the wave period  $T$  was estimated as the time difference between two points where the surface elevation is 1% of the amplitude of the wave.

### 5.4. Wave periods of the waves generated using the bottom-tilting wave maker

Figure 9 shows the wave peak time  $T_a$  plotted as a function of  $a$  and  $b$  for both upward and downward motions. It is observed that greater bottom motion duration  $b$  results in greater wave peak time  $T_a$ . However, dependence of  $T_a$  on  $a$  is different according to the direction of bottom movements. More specifically, while  $T_a$  decreases with  $a$  for upward motions, the opposite trend is found for downward motions. This interesting observation may be attributed to the nonlinear effects of the deformation of the wave profile. For upward motions, water surface elevation increases from the beginning of the wave to the peak, and the local wave celerity also increases with the surface elevation. Therefore the wave form

becomes squeezed and this tendency would be stronger for higher-amplitude waves. On the other hand, water surface elevation decreases from the beginning to the (negative) peak of the waves generated by the downward motions, and the wave form will be elongated at least up to the peak. Of course, this nonlinear effect cannot be expected from the linear analytic solution, which shows no functional dependence of  $T_a$  on  $a$ .

Wave periods estimated from the Boussinesq equations in semi-infinite domain are plotted against  $a$  and  $b$  in figure 10. Small-amplitude waves ( $a = 0.1$ ) are more or less symmetric, and their wave periods can also be estimated using the peak time, that is  $T = 2T_a$  (marked with star in figure 10). As in the case for the wave peak time, the wave period also increases with the bottom motion duration  $b$ . Dependence of the wave period on the bottom motion amplitude is, however, much more complicated. Unlike the peak time, now it is observed that the wave period increases monotonically with the motion amplitude for the waves generated by the upward motions. This is only explained if the waves are skewed with long tails so that  $T > 2T_a$ , which is also due to nonlinearity.

Wave periods of the waves generated by the downward motions no longer show monotonic dependence on  $a$ . For small motion amplitudes, the increase of peak time with  $a$  is almost cancelled due to the opposite trend of the tail. For larger amplitudes, dispersion manifests itself as disintegration of the wave form, which effectively reduces the wave period (see second and third panels of figure 5 (a) and (b)). After sudden decrease of the wave period, the nonlinear effects come into play again, and the wave period starts to increase with increasing  $a$  just like the waves generated by the upward motions.

Due to the rather complex response of the wave periods to the motion amplitudes, a simple functional description of  $T$  with respect to  $a$  and  $b$  could not be found. More investigation is needed to elucidate the roles of competing mechanism of nonlinearity and dispersion on wave periods of the long waves generated in the bottom-tilting wave maker.

## 6. Further discussion

So far, characteristics of the waves generated by the bottom-tilting wave maker, namely the wave amplitude and the wave period, have been discussed in terms of the parameters ( $a$  and  $b$ ) of simple upward and downward bottom motions. In this section, we further investigate the new wave maker. First of all, the waves generated in the new wave tank are compared to the relevant solitary waves, demonstrating that the new wave maker can indeed generate waves that are longer than the solitary waves. Then the bottom-tilting-generated wave is compared to the field data of 2011 Japan Tohoku tsunami. Finally, the effects of the length of the tilting bottom are also discussed.

Figure 11 illustrates the comparison of the ratio  $L_w/L_s$  of wave length between the solitary waves and the bottom-tilting generated waves for  $\alpha = 0.05$ . The ratio  $L_w/L_s$  is always greater than 1, demonstrating that the bottom-tilting wave maker can generate waves longer than the solitary waves. Also notice that the  $L_w/L_s$  mostly grows with increasing motion amplitude and with increasing motion duration, except some sudden drop due to dispersion for downward motion.

The field data of the 2011 Japan Tohoku tsunami shown in figure 12 (a) by solid line was

obtained at a location with a water depth of 204 m. The amplitude of the leading wave was 6.6 m and the wave period was 1500 s [Fujii *et al.*, 2011], resulting in the normalised wave amplitude ( $A_t$ ) to be  $A_t = 0.032$ . The upward bottom motion in the new wave maker with  $a = 0.1$  and  $b = 1.40$  just satisfies  $A = 0.032$ , and the result (dash-dotted) is compared to the field data (solid) as shown in figure 12 (a). The corresponding wave period of the bottom-tilting-generated wave is still shorter than the field data, albeit much better than the solitary wave (dotted). However, closer inspection of the figure shows that the wave agrees well with the field data near the peak of the tsunami record. It is an encouraging result considering that we only used a simple upward motion and suggests that more sophisticated operation of the tilting bottom should be able to achieve better agreement with the field data. Theoretically, if the wave is allowed to propagate by applying the bottom motion displacement  $\zeta(x = 0, t)$  (solid) as shown in figure 12 (b), the new wave maker is able to generate a wave (dashed) that is very similar to the field data as shown in figure 12 (a). Furthermore, the time histories of the motion displacement  $a$  and the relative motion speed  $Q$  determined by Eq. (4) are described in figure 12 (b) as well.

The wavelengths of the bottom-tilting-generated waves are mainly limited by the length of the tilting bottom and limited motion tested. Previously, in section 3, we showed that the length of the tilting bottom relative to the water depth plays an important role in determining the characteristics of the resulting waves. In figure 13, the dependence of wave amplitude and wave period on the tilting bottom length is plotted. It can be seen that increasing length of the moving bottom leads to growing wave amplitude but decreasing (dimensionless) period for both kinds of bottom motions.

## 7. Conclusions

In this paper, we have presented our new wave maker, namely the bottom-tilting wave maker, which can generate waves that are significantly longer than solitary waves. This was motivated by recent advancement in tsunami research [e.g. Madsen *et al.*, 2008], which points out that use of solitary waves to model tsunamis is not theoretically justified.

By changing the water depth, bottom motion displacement and speed, different waves have been created and investigated. The amplitudes and the periods of the generated waves were related to the parameters of the simple bottom motions. The wave amplitudes are well described in terms of the volume flux of the displaced water, but the wave periods show much more complicated trends due to combined effects of nonlinearity and dispersion.

With one moving bottom in simple monotonic motions, we were able to generate waves that are markedly similar to the field data of 2011 Japan Tohoku tsunami. We expect that more sophisticated operation would result in even better agreement. This wave maker effectively changes the length of moving bottom and provides more degrees-of-freedom in operation.

## 14 REFERENCES

377 **Acknowledgements**

378 YSP acknowledges financial support from the Royal Society of Edinburgh through the  
 379 Royal Society of Edinburgh and Scottish Government Personal Research Fellowship Co-  
 380 Funded by the Marie-Curie Actions. This research is also supported by the financial sup-  
 381 port from the Korea Institute of Marine Science and Technology Promotion [Reference No.  
 382 20140437].

383 **References**

- 384 Aránguiz, R., González, G., González, J., Catalán, P. A., Cienfuegos, R., Yagi, Y., Okuwaki,  
 385 R., Urrea, L., Contreras, K., Del Rio, I. *et al.* [2016] The 16 september 2015 chile tsunami  
 386 from the post-tsunami survey and numerical modeling perspectives, *Pure and Applied*  
 387 *Geophysics* **173**(2), 333–348.
- 388 Boussinesq, J. [1872] Théorie des ondes et des remous qui se propagent le long d’un canal  
 389 rectangulaire horizontal, en communiquant au liquide contenu dans ce canal des vitesses  
 390 sensiblement pareilles de la surface au fond. *Journal de Mathématiques Pures et Ap-*  
 391 *pliquées*, 55–108.
- 392 Fujii, Y., Satake, K., Sakai, S., Shinohara, M. and Kanazawa, T. [2011] Tsunami source  
 393 of the 2011 off the pacific coast of tohoku earthquake, *Earth, planets and space* **63**(7),  
 394 815–820.
- 395 Fujima, K., Achmad, F., Shigihara, Y. and Mizutani, N. [2009] Estimation of tsunami force  
 396 acting on rectangular structures, *Journal of Disaster Research* **4**(6), 404–409.
- 397 Goring, D. G. [1978] *Tsunamis—the propagation of long waves onto a shelf*, PhD thesis,  
 398 California Institute of Technology.
- 399 Goseberg, N., Wurpts, A. and Schlurmann, T. [2013] Laboratory-scale generation of  
 400 tsunami and long waves, *Coastal Engineering* **79**, 57–74.
- 401 Hall, J. V. J. and Watts, G. M. [1953] Laboratory investigation of the vertical rise of solitary  
 402 waves on impermeable slopes, Tech. rep., U.S. Beach Erosion Board.
- 403 Hammack, J. L. [1973] A note on tsunamis: their generation and propagation in an ocean  
 404 of uniform depth, *J. Fluid Mech.* **60**(04), 769–799, doi:10.1017/s0022112073000479,  
 405 <http://dx.doi.org/10.1017/S0022112073000479>.
- 406 Harten, A. and Osher, S. [1987] Uniformly high-order accurate nonoscillatory schemes.  
 407 i, *SIAM J. Numer. Anal.* **24**(2), 279–309, doi:10.1137/0724022, [http://dx.doi.org/](http://dx.doi.org/10.1137/0724022)  
 408 [10.1137/0724022](http://dx.doi.org/10.1137/0724022).
- 409 Hayashi, Y., Tsushima, H., Hirata, K., Kimura, K. and Maeda, K. [2011] Tsunami source  
 410 area of the 2011 off the pacific coast of tohoku earthquake determined from tsunami  
 411 arrival times at offshore observation stations, *Earth, Planets and Space* **63**(7), 54, doi:  
 412 [10.5047/eps.2011.06.042](http://dx.doi.org/10.5047/eps.2011.06.042), <http://dx.doi.org/10.5047/eps.2011.06.042>.
- 413 Kihara, N., Niida, Y., Takabatake, D., Kaida, H., Shibayama, A. and Miyagawa, Y. [2015]  
 414 Large-scale experiments on tsunami-induced pressure on a vertical tide wall, *Coastal*  
 415 *Engineering* **99**, 46–63.
- 416 Li, Y. and Raichlen, F. [2002] Non-breaking and breaking solitary wave run-up, *J.*

- 417 *Fluid Mech.* **456**, 295–318, doi:10.1017/s0022112001007625, [http://dx.doi.org/](http://dx.doi.org/10.1017/S0022112001007625)  
418 [10.1017/S0022112001007625](http://dx.doi.org/10.1017/S0022112001007625).
- 419 Lo, H.-Y., Park, Y. S. and Liu, P. L.-F. [2013] On the run-up and back-wash processes of  
420 single and double solitary wavesan experimental study, *Coastal engineering* **80**, 1–14.
- 421 Lu, H., Park, Y. S. and Cho, Y.-S. [2017] Modelling of long waves generated by bottom-  
422 tilting wave maker, *Coastal Engineering* **122**, 1–9.
- 423 Madsen, P. A., Fuhrman, D. R. and Schäffer, H. A. [2008] On the solitary wave paradigm  
424 for tsunamis, *J. Geophys. Res.* **113**(C12012), doi:10.1029/2008jc004932, [http://dx.](http://dx.doi.org/10.1029/2008JC004932)  
425 [doi.org/10.1029/2008JC004932](http://dx.doi.org/10.1029/2008JC004932).
- 426 Mei, C. C. [1989] *The Applied Dynamics of Ocean Surface Waves* (World scientific).
- 427 O'Donoghue, T., Pokrajac, D. and Hondebrink, L. [2010] Laboratory and numerical  
428 study of dambreak-generated swash on impermeable slopes, *Coastal Engineering*  
429 **57**(5), 513 – 530, doi:<http://dx.doi.org/10.1016/j.coastaleng.2009.12.007>, [http://www.](http://www.sciencedirect.com/science/article/pii/S0378383909002166)  
430 [sciencedirect.com/science/article/pii/S0378383909002166](http://www.sciencedirect.com/science/article/pii/S0378383909002166).
- 431 Rossetto, T., Allsop, W., Charvet, I. and Robinson, D. I. [2011] Physical modelling of  
432 tsunami using a new pneumatic wave generator, *Coastal Engineering* **58**(6), 517–527.
- 433 Schimmels, S., Sriram, V. and Didenkulova, I. [2016] Tsunami generation in a large scale  
434 experimental facility, *Coastal Engineering* **110**, 32–41.
- 435 Shu, C.-W. [1998] Essentially non-oscillatory and weighted essentially non-oscillatory  
436 schemes for hyperbolic conservation laws, A. Quarteroni (ed.), *Advanced Numeri-*  
437 *cal Approximation of Nonlinear Hyperbolic Equations*, Lecture Notes in Mathematics,  
438 Vol. 1697 (Springer Berlin Heidelberg), ISBN 978-3-540-64977-9, pp. 325–432, doi:  
439 [10.1007/BFb0096355](http://dx.doi.org/10.1007/BFb0096355), <http://dx.doi.org/10.1007/BFb0096355>.
- 440 Synolakis, C. E. [1987] The runup of solitary waves, *J. Fluid Mech.* **185**, 523–545, doi:  
441 [10.1017/S002211208700329x](http://dx.doi.org/10.1017/S002211208700329x), <http://dx.doi.org/10.1017/S002211208700329x>.
- 442 Tsuji, Y., Namegaya, Y., Matsumoto, H., Iwasaki, S.-I., Kanbua, W., Sriwichai, M. and  
443 Meesuk, V. [2006] The 2004 indian tsunami in thailand: Surveyed runup heights and  
444 tide gauge records, *Earth, Planets and Space* **58**(2), 223–232, doi:10.1186/BF03353382,  
445 <http://dx.doi.org/10.1186/BF03353382>.
- 446 Walder, J. S., Watts, P., Sorensen, O. E. and Janssen, K. [2003] Tsunamis generated by  
447 subaerial mass flows, *Journal of Geophysical Research: Solid Earth* **108**(B5).
- 448 Wu, T. Y.-T. [1987] Generation of upstream advancing solitons by moving disturbances, *J.*  
449 *Fluid Mech.* **184**, 75–99.



## 16 REFERENCES

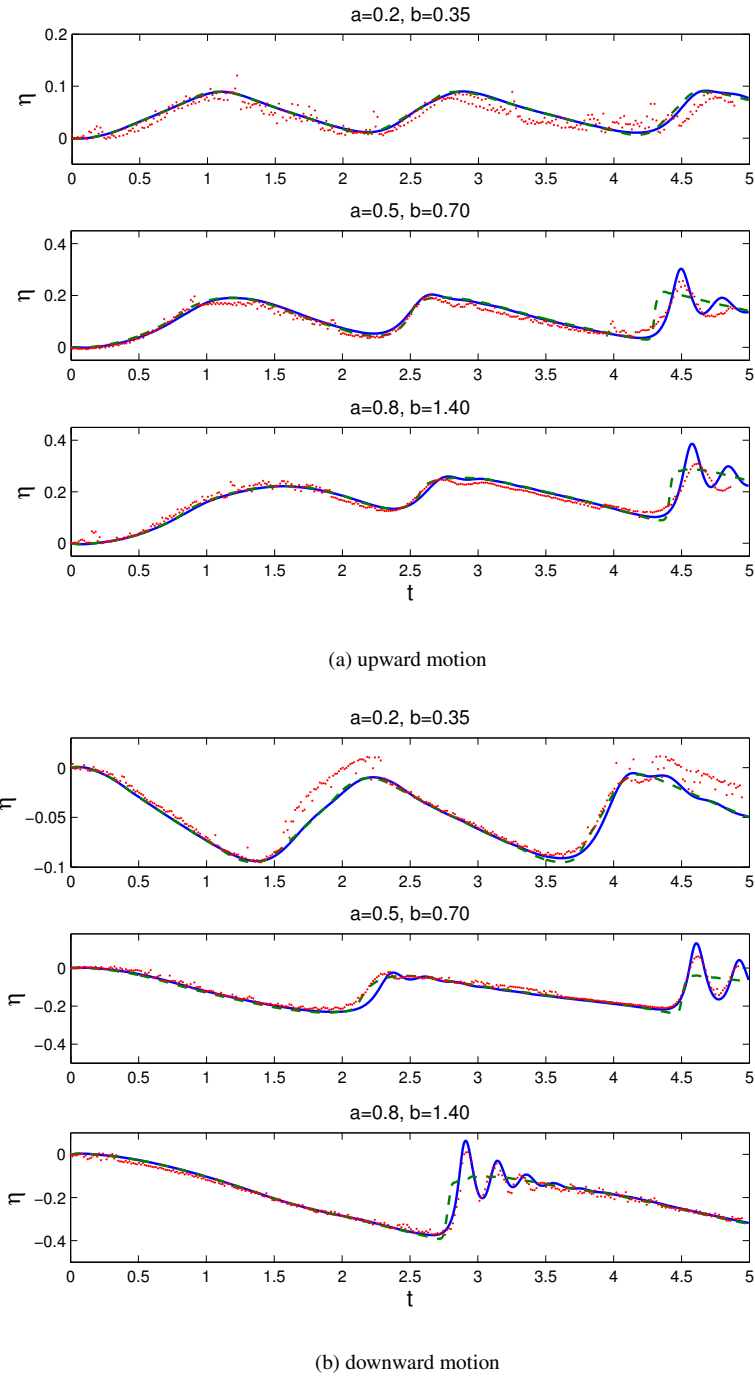


Fig. 5. Comparison of the free surface elevation at the hinge: solid line, numerical results by BE; dashed line, numerical results by NSW; dotted line, experimental data.

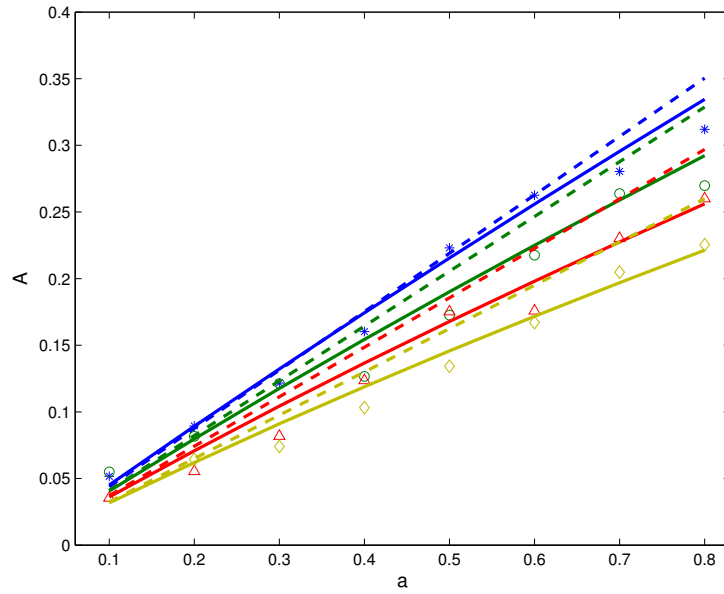
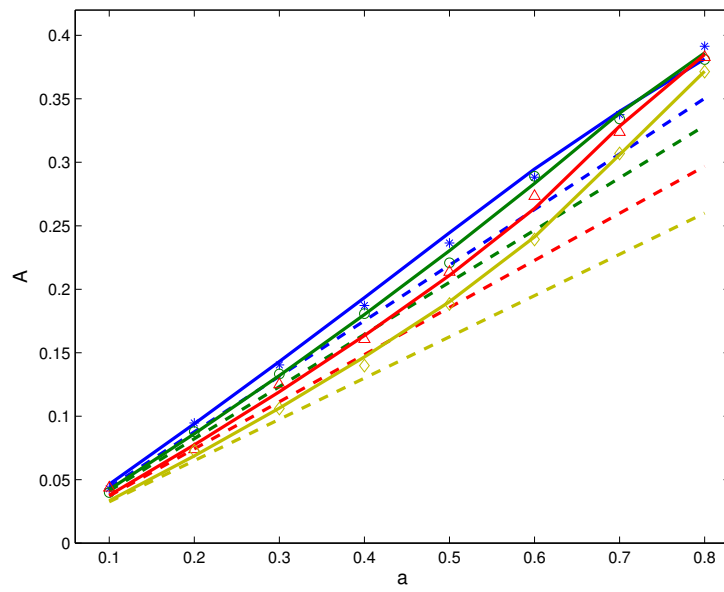
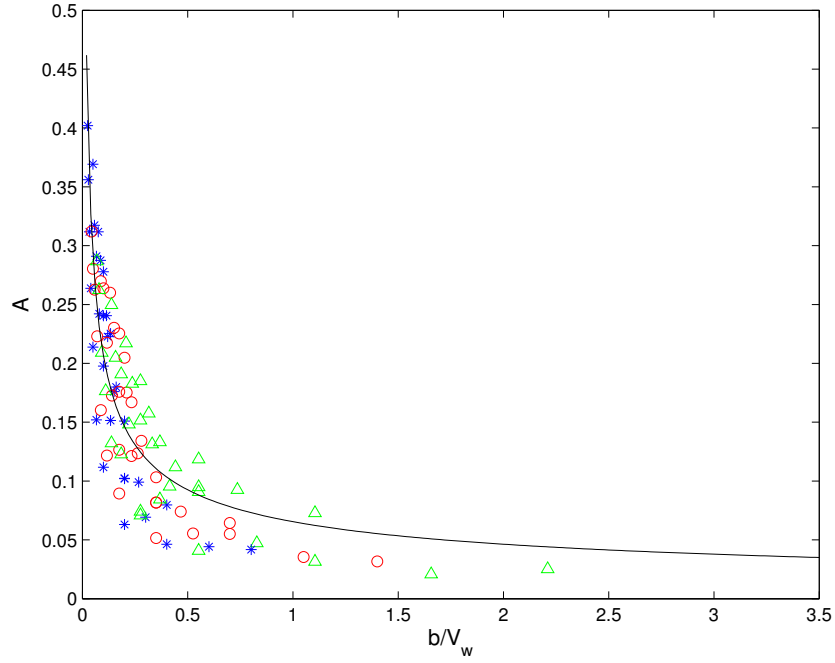
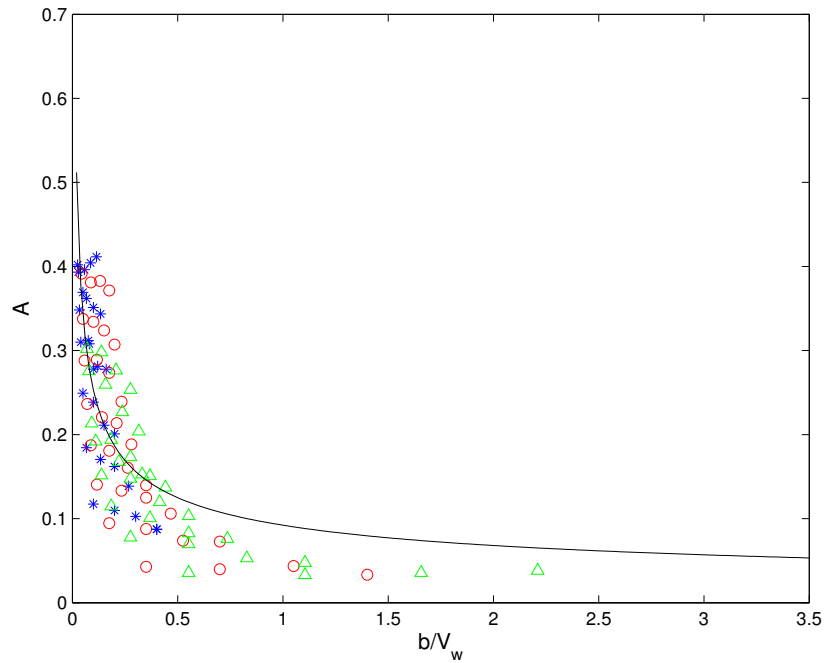
(a) Amplitude  $A$  for upward motions(b) Amplitude  $A$  for downward motions

Fig. 6. Effects of bottom motion on wave amplitude of the waves generated in the wave maker: \*,  $b = 0.35$ ;  $\circ$ ,  $b = 0.70$ ;  $\triangle$ ,  $b = 1.05$ ;  $\diamond$ ,  $b = 1.40$ ; solid line, numerical results by BE; dashed line, analytical results by linear wave theory (lines are distinguished following the symbols from top to bottom).

## 18 REFERENCES

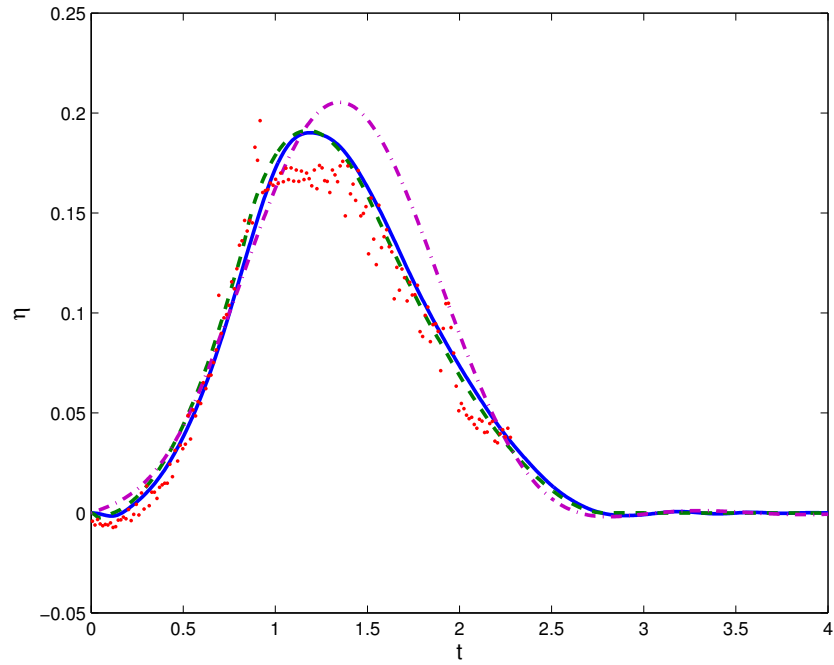


(a) upward motion

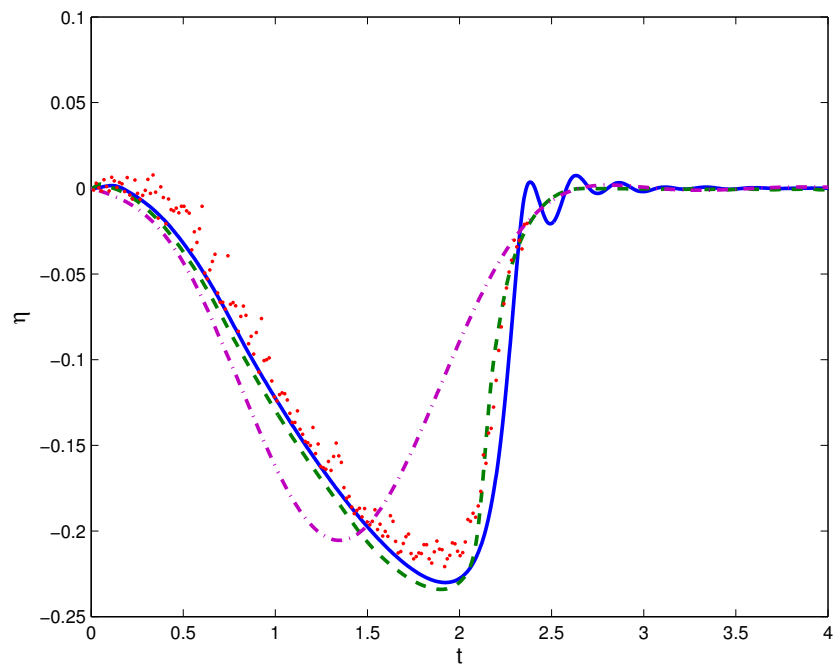


(b) downward motion

Fig. 7. Plots of wave amplitude  $A$  as functions of  $b/V_w$ : solid line, the fitting function; \*,  $\alpha = 0.04$ ;  $\circ$ ,  $\alpha = 0.05$ ;  $\triangle$ ,  $\alpha = 0.06$ .



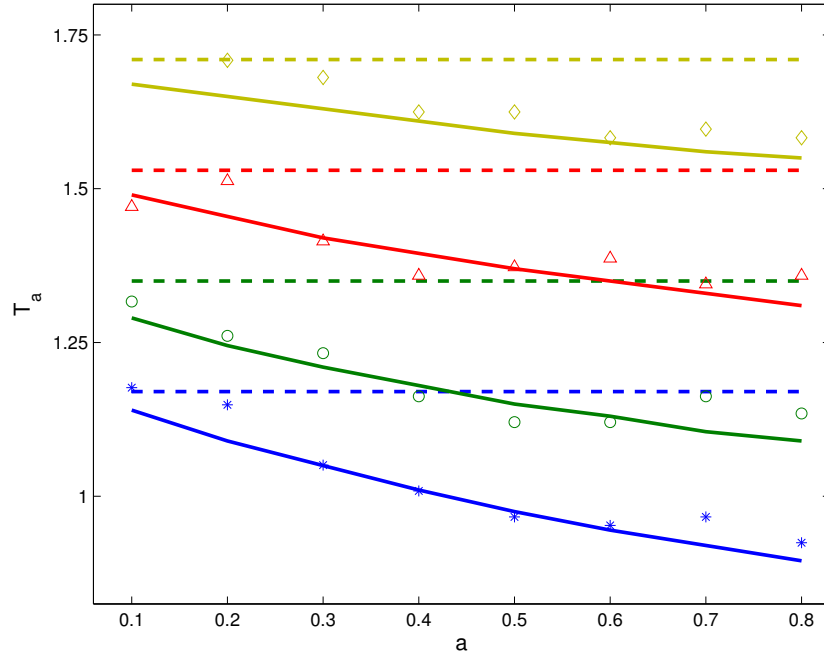
(a) upward motion



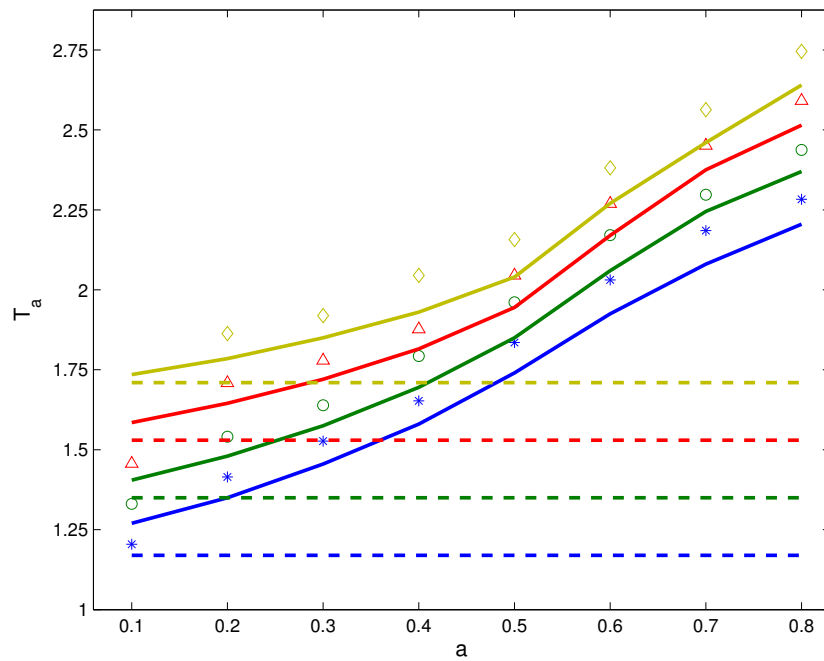
(b) downward motion

Fig. 8. Theoretical results for waves in semi-infinite domain compared to experimental data: solid line, results by BE; dashed line, results by NSWE; dash dotted line, linear analytical results; dot, experimental data.

20 REFERENCES



(b) Peak time  $T_a$  with varying bottom motions



(b) Peak time  $T_a$  with varying bottom motions

Fig. 9. Effects of bottom motion on wave peak time  $T_a$  of the resulting waves: \*,  $b = 0.35$ ;  $\circ$ ,  $b = 0.70$ ;  $\triangle$ ,  $b = 1.05$ ;  $\diamond$ ,  $b = 1.40$ ; solid line, numerical results by BE; dashed line, analytical results by linear wave theory (lines are distinguished following the symbols from top to bottom).

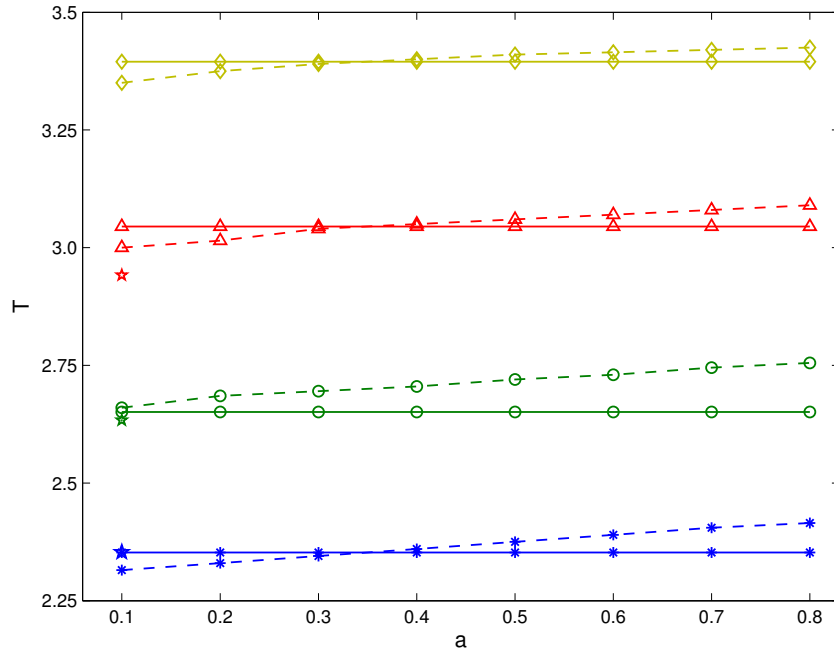
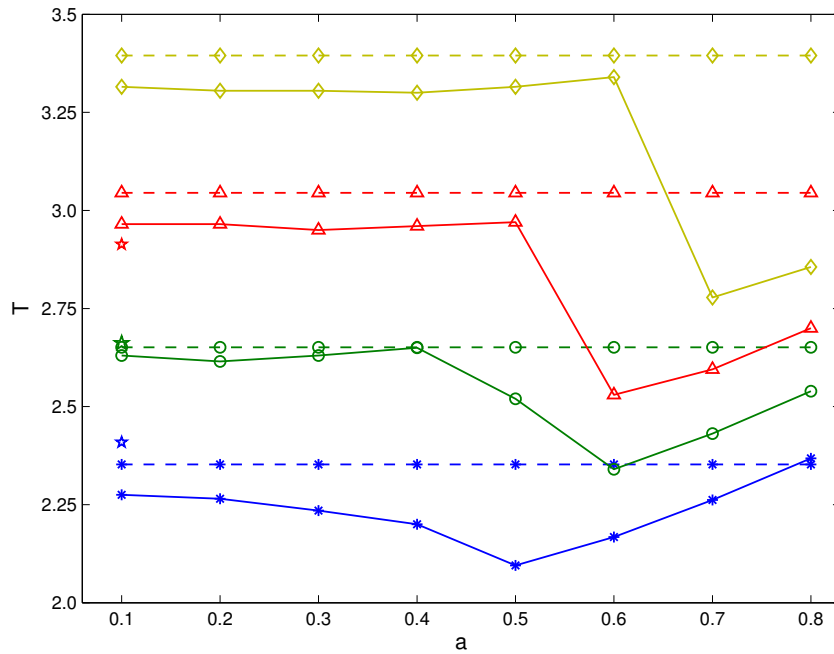
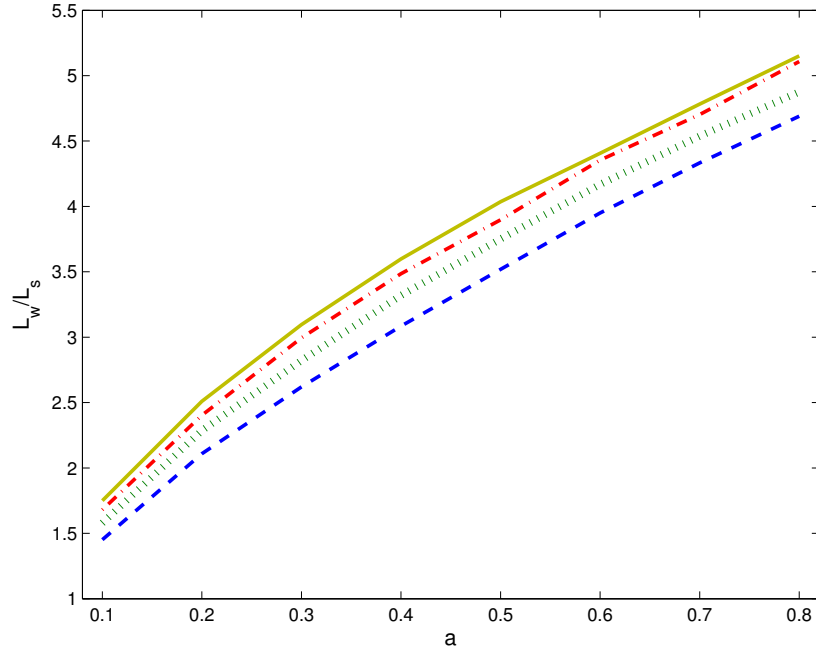
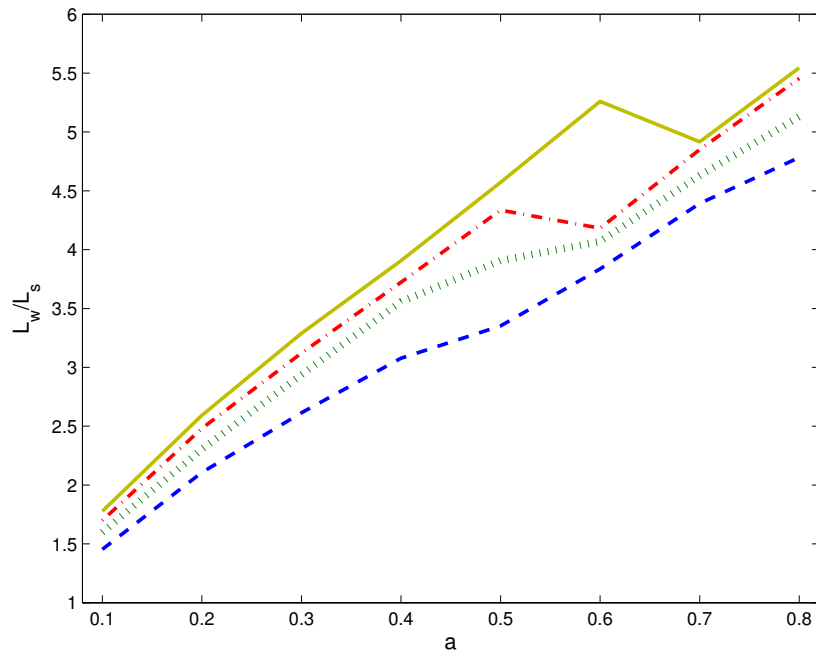
(a) Period  $T$  with varying  $a$  for upward motion(b) Period  $T$  with varying  $a$  for downward motion

Fig. 10. Effects of bottom motion on wave period of the resulting waves: \*,  $b = 0.35$ ;  $\circ$ ,  $b = 0.70$ ;  $\triangle$ ,  $b = 1.05$ ;  $\diamond$ ,  $b = 1.40$ ; solid line, numerical results by BE; dashed line, analytical results by linear wave theory;  $\star$ , experimental data (adjacent to its corresponding  $b$ ).

## 22 REFERENCES

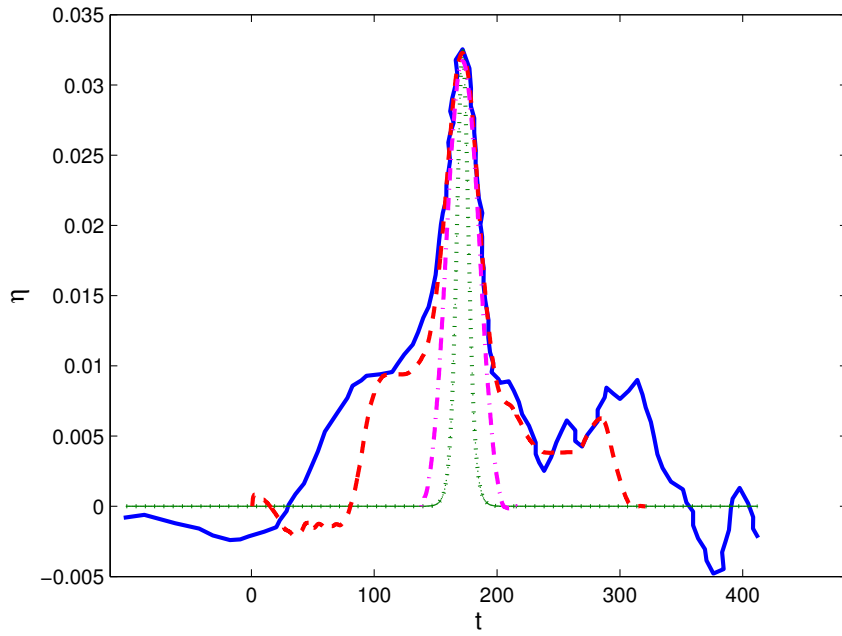


(a) upward motion

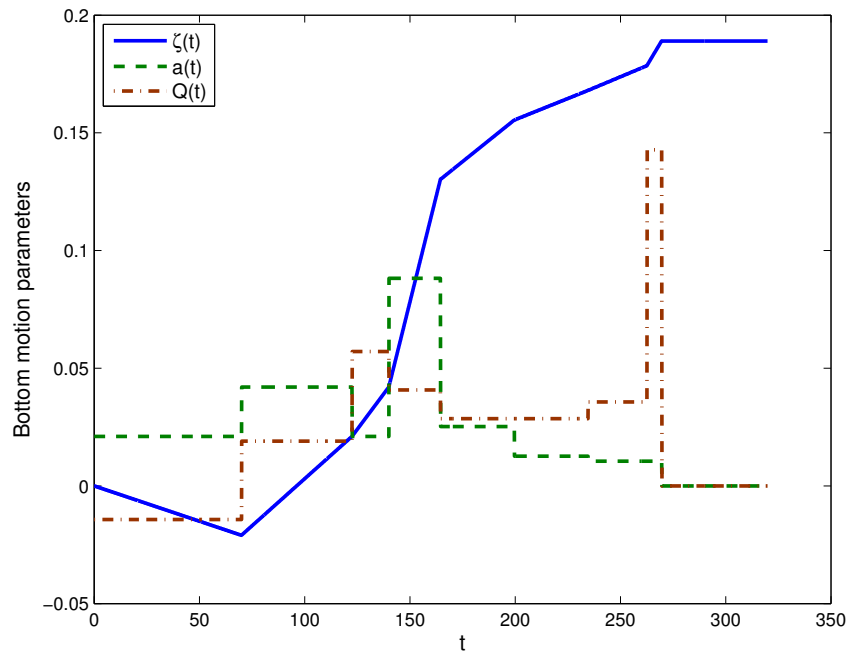


(b) downward motion

Fig. 11. Comparison of the ratio of  $L_w/L_s$  with varying  $a$  and  $b$  for upward motion and downward motion: dashed line,  $b = 0.35$ ; dotted line,  $b = 0.70$ ; dash dotted line,  $b = 1.05$ ; solid line,  $b = 1.40$ .



(a) Comparison between field data and fitted waves: solid line, the observed field data; dashed line, the wave generated by a sophisticated bottom motion; dash dotted line, the wave generated by a simple upward motion; dotted line, the fitted solitary wave .

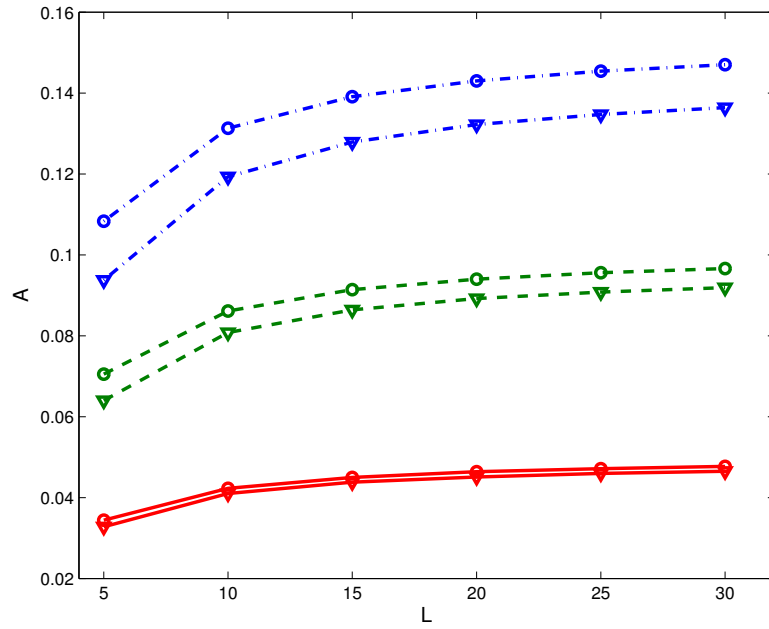


(b) Bottom motion parameters  $\zeta(x=0, t)$  (solid line),  $Q(t)$  (dash dotted line) and  $a(t)$  (dashed line) of the fitted wave by a sophisticated bottom motion

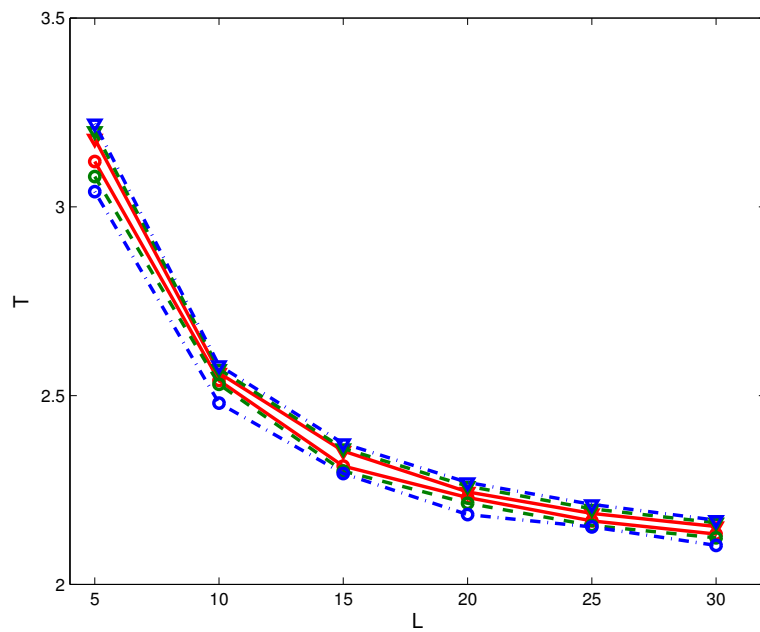
Fig. 12. Comparison between field data at Iwate South from Japan Tohoku tsunami in 2011 (Fujii *et al.* [2011]), fitted bottom-tilting-generated waves and a fitted solitary wave.



## 24 REFERENCES



(a) wave amplitude



(b) wave period

Fig. 13. Comparison of wave characteristics with varying moving bottom length:  $\nabla$ , upward motion;  $\circ$ , downward motion; solid line,  $a = 0.1$ ; dashed line,  $a = 0.2$ ; dash dotted line,  $a = 0.3$ .